communications earth & environment

Article

A Nature Portfolio journal

https://doi.org/10.1038/s43247-025-03105-3

Detrital zircon–apatite fingerprinting challenges glacial transport of Stonehenge's megaliths

Check for updates

Anthony J. I. Clarke ✉ & Christopher L. Kirkland

How Stonehenge's building blocks arrived on Salisbury Plain remains debated, with glacial and human transport mechanisms proposed. Here we test the possibility of Pleistocene glacial sediment input using grain-scale U–Pb fingerprinting of detrital zircon and apatite from modern stream sediments surrounding Stonehenge. Zircon ages span 3396–285 Ma, with age peaks at ~1090, 1690, and 1740 Ma, matching the Laurentian basement of northern Britain. Salisbury Plain detrital zircon ages match those of southern British rocks sourced from the London Basin, implying local sediment recycling rather than glaciogenic transport. Apatite ages of ~60 Ma reflect post-depositional U–Pb resetting, consistent with the distal effects of the Alpine orogeny. Collectively, our data show Salisbury Plain remained unglaciated during the Pleistocene, making direct glacial transport of Stonehenge's megaliths unlikely.

The isotopic and chemical analysis (e.g. U–Pb and trace elements) of detrital grains, such as zircon and apatite, represents a versatile tool in tracing sediment flux[1–3], provenance[4–6], and regolith formation[7–9]. Resistant detrital grains in modern stream sediments may reflect direct source to sink pathways or more complex, multi-cycle transport histories, given the refractory nature of these heavy minerals under certain physical and chemical conditions[10–12].

The relative contributions of direct versus recycled detrital sources to regolith and sedimentary rocks throughout Britain have been highlighted in the scientific literature, although regional and inter-basin variability remains unresolved[13–16]. Clarifying sediment transport pathways can help inform paleogeographic reconstructions and basin evolution[3,17,18]. Moreover, resolving source-to-sink relationships can contribute to provenance debates in archaeological science[19,20], including whether megaliths on Salisbury Plain, England (Fig. 1), were transported by glacial processes or human agency.

Salisbury Plain, England, represents a rich Neolithic archaeological landscape, including monumental architecture at Stonehenge and Avebury[21]. Megaliths at Stonehenge form three groups. The largest are the ca. 25-tonne sarsen stones, composed of silcrete, which form the lintelled outer circle and inner trilithon horseshoe. The sarsen stones are comparatively local; most were sourced from West Woods, ca. 25 km from Stonehenge[22,23]. The bluestones, sourced from approximately 230 km away in the Mynydd Preseli in Wales, weigh between 2 and 5 tonnes and comprise an assemblage of volcanic and sedimentary rocks, including tuff, rhyolite, and dolerite[24]. The Mynydd Preseli bluestones yield Darriwilian (464–462 Ma) zircon U–Pb ages[25]. The third megalith type is the Altar Stone, a single six-tonne slab of Palaeozoic Old Red Sandstone (ORS)[26,27]. Recent research suggests the Altar Stone originated in the Orcadian Basin of northeast Scotland, over 700 km from Stonehenge (Fig. 1)[26].

Salisbury Plain is a chalk plateau covering ca. 775 km^2 in southern England (Fig. 1). Stratigraphically, the plateau is dominated by Upper Cretaceous Chalk (Turonian–Maastrichtian, approximately 93–66 Ma), overlying gently dipping Lower Cretaceous and Upper Jurassic formations (approximately 152–145 Ma) that include mudstones, sandstones, and limestones[28,29]. Prior to Neogene erosion, Paleogene sediments once covered much of the Salisbury Plain plateau, with remnant rocks persisting locally as relict units, including the Clay-with-Flints deposits[28–30] (Fig. 1). River valleys (e.g. the Avon, Wylye, and Bourne) define the plain's margins and dissect stratigraphy to expose older Mesozoic rocks, comprising mudstones, sandstones, limestones, and locally fossiliferous horizons deposited in shallow marine to fluvial environments[29,31] (Fig. 1). Salisbury Plain exhibits low-amplitude relief, with elevations between 100 and 250 m above sea level, and is drained by a dendritic network of rivers, including the Avon, Wylye, and Bourne, which flow towards the south and southeast (Fig. 1).

The origin of the non-sarsen building blocks of Stonehenge on Salisbury Plain is debated. Most suggest that Neolithic people transported the bluestones from the Mynydd Preseli and Orcadian Basin to Salisbury Plain via overland or sea routes[26,32,33] (Fig. 1). An alternative view, the glacial transport hypothesis, posits that non-sarsen megaliths, including the Mynydd Preseli bluestones and the Altar Stone, were transported to Salisbury Plain as erratics during Pleistocene glaciations. The case for glacial transport of megaliths principally rests on geomorphological arguments that pre-Devensian ice streams (e.g. Anglian

Timescales of Mineral Systems Group, School of Earth and Planetary Sciences, Curtin University, Perth, WA, Australia. ✉e-mail: 287729e@curtin.edu.au

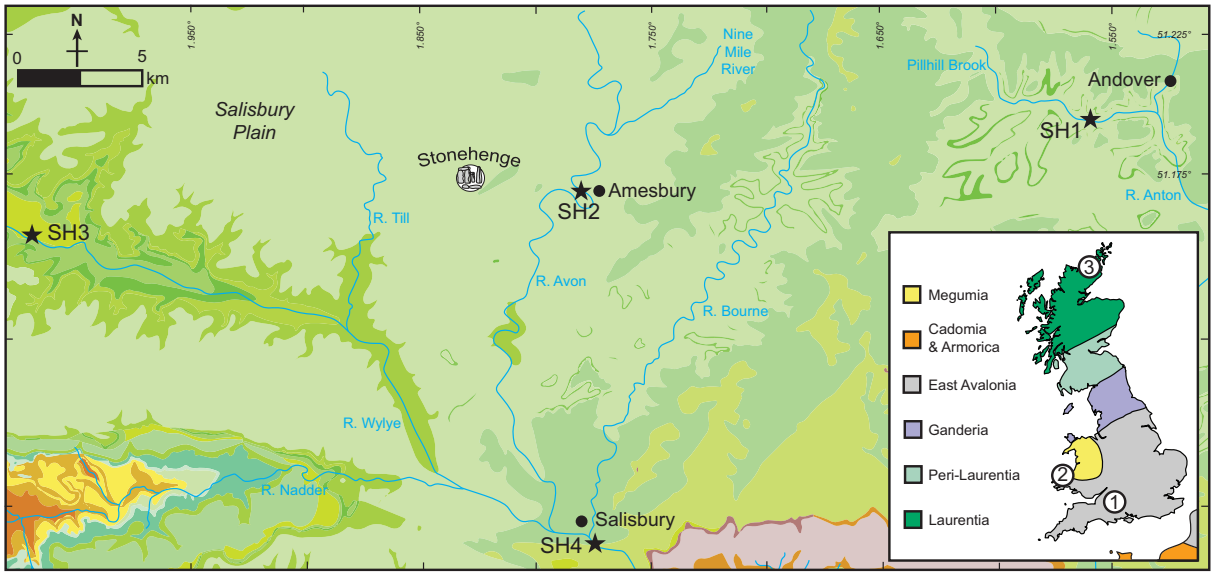

SEAFORD CHALK FORMATION
LEWES NODULAR CHALK FORMATION
NEWHAVEN CHALK FORMATION
WEST MELBURY MARLY CHALK
READING FORMATION
WITTERING FORMATION
LONDON CLAY FORMATION
DURLSTON LIMESTONE FORMATION
LULWORTH LIMESTONE FORMATION
TISBURY LIMESTONE MEMBER
GAULT MUDSTONE FORMATION
STOCKBRIDGE LIMESTONE

Period	Epoch	Lithostratigraphic Units		Thickness (m)
QUATERNARY	PLEISTOCENE TO HOLOCENE	Head Gravelly Head Clay-with-flints Peat Alluvium Fisherton Brickearth River Terrace Deposits		1-10
PALAEOGENE	EOCENE	BRACKLESHAM GROUP	WITTERING FM.	5-15
		THAMES GROUP	LONDON CLAY FM.	35-50
	PALAE-OCENE	LAMBETH GROUP	THANET & READING FMS.	15-30
CRETACEOUS	LATE	WHITE CHALK SUBGROUP	PORTSDOWN CHALK FM.	5-10
			CULVER CHALK FM.	35-45
			NEWHAVEN CHALK FM.	55-70
			SEAFORD CHALK FM.	60-70
			LEWES NODULAR CHALK FM.	40-45
			NEW PIT CHALK FM.	25-35
			HOLYWELL NODULAR CHALK FM.	15-25
		GREY CHALK SUBGROUP	ZIG ZAG CHALK FM.	46-65
			WEST MELBURY MARLY CHALK FM.	25-40

CRETACEOUS	EARLY	UPPER GREENSAND FORMATION GAULT MUDSTONE FORMATION		35-75 25-58
		LOWER GREENSAND GROUP	UNDIVIDED	up to 20
		WEALDEN GROUP	UNDIVIDED	up to 10
JURASSIC	LATE	PURBECK GROUP	DURLSTON FM. LULWORTH FM.	up to 13 up to 15
		PORTLAND GROUP	TISBURY LIMESTONE MBR. PORTLAND SAND	12-15 up to 19
		KIMMERIDGE CLAY FORMATION		184-273 (up to 10 at outcrop)
		CORALLIAN GROUP		43-51
	MIDDLE	OXFORD CLAY FM. KELLAWAYS FM.		135-190
		GREAT OOLITE GROUP		118-180
		INFERIOR OOLITE GROUP		15-42
	EARLY	LIAS GROUP		256-430
PERMIAN TO JURASSIC		PENARTH GROUP MERCIA MUD-STONE GROUP SHERWOOD SAND STONE GROUP		120-286
CARBONIFEROUS TO CAMBRIAN				

Fig. 1 | A simplified geological map and stratigraphic column of Salisbury Plain, England. Black stars indicate the location of stream sand sample sites. Coordinates are in decimal degrees. Stream sediment sampling sites (SH1–SH4) are located within the Avon–Test drainage system catchments, as illustrated by the regional hydrology shown by blue lines. The inset shows the major basement terranes of Britain and northern France[96]. Circled numbers show key locations discussed, including: 1. Stonehenge, 2. Mynydd Preseli and 3. the Orcadian Basin of northeast mainland Scotland. The geodetic system used is WGS 84.

or Wolstonian) may have extended farther south toward Salisbury Plain, and on reports of isolated boulders in southern England inferred to be of Welsh origin[34–36].

The absence, ambiguity, or inaccessibility of purported glacial features on Salisbury Plain hampers efforts to reconstruct potential ice flow and erratic transport pathways[34,37]. Thus, based on current evidence, it is difficult to resolve whether ice ever covered all or part of Salisbury Plain during pre-Devensian glaciations. Nonetheless, the maximum extent of the Anglian Stage glaciation (ca. 478–424 ka) in central southern Britain remains poorly constrained[38], although no diagnostic evidence demonstrates direct glacial incursion onto the Plain itself[35,36]. Outwash from glaciers can transport fine detrital grains (typically <200 μm) well beyond the terminal margins of ice sheets, whereas larger erratics, often ranging from tens of centimetres to several metres, are typically deposited closer to the ice front[39,40]. In both cases, glacial sediment transport is expected to leave persistent and detectable provenance signatures, preserved in the landscape as indicators of sediment routing and crystalline source regions following ice retreat[40,41].

Geochemical data for detrital minerals offer a novel test of the competing anthropogenic versus glacial transport hypotheses. If glacial erratics had reached Salisbury Plain, they would be expected to contribute a substantial ca. 464 Ma zircon population from Mynydd Preseli source rocks[25] in southwest Wales or Ganderian-Laurentian signatures from northern Britain into the local sediment budget (Fig. 1). Given the Chalk's low zirconium content, most detrital zircon is unlikely to be locally derived. Instead, detrital zircon grains in stream sediment are more plausibly sourced from zircon-rich crystalline lithologies beyond the plain, with glacial processes representing one potential transport mechanism[40]. In contrast, apatite could plausibly derive from phosphorite horizons within the Chalk surrounding Stonehenge[42,43]. In any case, a combined zircon-apatite approach provides a more comprehensive means of distinguishing between first-cycle from multi-cycle detritus and post-depositional processes[44–46].

Here, we report U–Pb isotopic data for detrital zircon and apatite collected from streams draining Salisbury Plain, England (Figs. 2 and 3) (Table 1). Our results demonstrate the widespread dispersal of multi-cycle Laurentian detritus across Britain. We utilise the detrital fingerprint of unconsolidated river sands to constrain potential glacial-sediment pathways, which have implications for the debate over the origins of the building blocks of Stonehenge, specifically whether they are of anthropogenic or ice-transported origin.

Results

Zircon U–Pb

U–Pb isotopic data were obtained from 550 individual zircon grains (Supplementary Data 1). Four hundred and one analyses are defined as concordant (<±10% discordant). Concordant zircon dates span 3396 ± 30–285 ± 5 Ma (Fig. 2), with coherent age peaks defined by ≥10 grains[47] ranging from the Silurian to Paleoproterozoic, including components at ca. 432 ($n = 16$), 447 ($n = 15$), 460 ($n = 11$), 1015 ($n = 21$), 1054 ($n = 22$), 1089 ($n = 30$), 1167 ($n = 13$), 1184 ($n = 15$), 1213 ($n = 11$), 1251 ($n = 10$), 1375 ($n = 10$), 1403 ($n = 10$), 1502 ($n = 13$), 1526 ($n = 15$), 1542 ($n = 11$), 1575 ($n = 11$), 1672 ($n = 18$), 1694 ($n = 23$), 1744 ($n = 24$), 1798 ($n = 13$), 1848 ($n = 23$), and 1870 Ma ($n = 22$).

Zircon morphology

Zircon grains exhibit elongate to sub-rounded shapes with aspect ratios ranging from ~2:1 to 5:1. Grains have a length up to ~250 μm, with most 50 μm long (Fig. 4). Cathodoluminescence imaging reveals a variety of internal zoning patterns consistent with a diverse, predominantly igneous sources, including oscillatory zoning (e.g. SH1.12, SH2.59), sector zoning (e.g. SH3.26), and rare examples of core-rim relationships suggestive of metamorphic overgrowths (e.g. SH1.19) (Fig. 4). Most grains show signs of rounding and abrasion, implying sedimentary transport and recycling. Complex internal structures, such as inherited cores (e.g. SH2.91), support derivation from crustal sources with variable mineral (re)growth events.

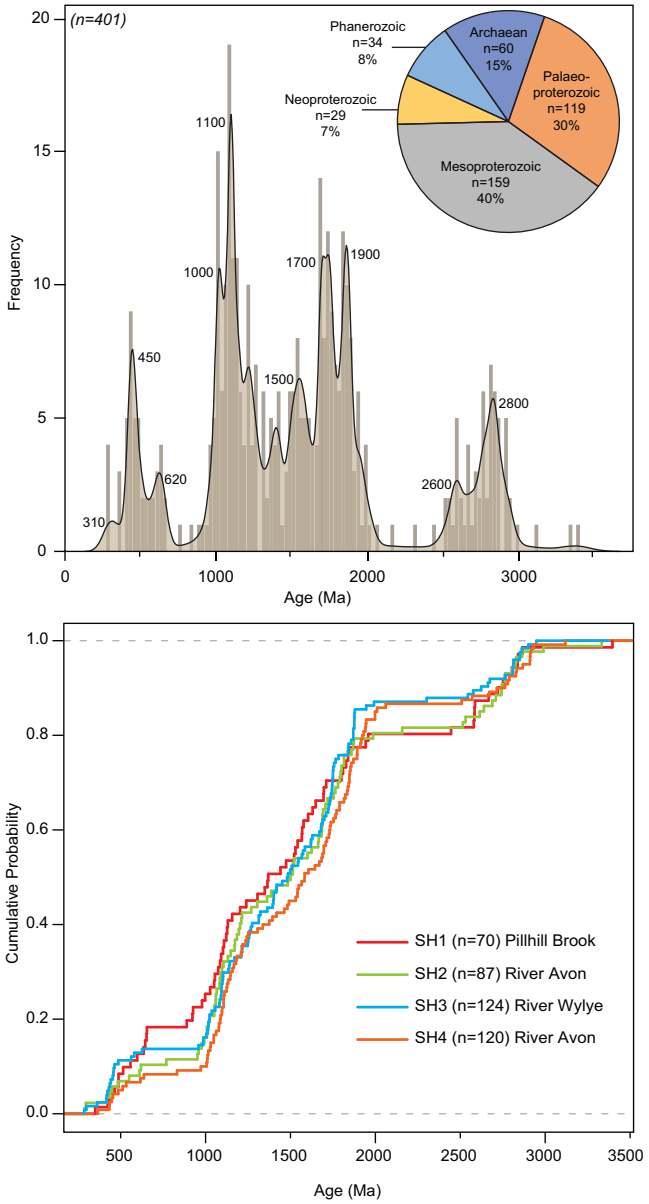

Fig. 2 | U–Pb data for detrital zircon from Salisbury Plain. *Top panel:* A kernel density plot of detrital zircon U–Pb ages from all stream sediment samples (SH1–SH4, total number of concordant grains = 401/550), plotted with 20 Ma bandwidths and overlaid with histogram bins. Peak age components occur at ca. 1100, 1700 Ma, and 1750 Ma[49]. The inset pie chart shows the proportion of concordant zircon analyses by age. *Bottom panel:* Cumulative probability plots for each sample location, colour-coded by stream and catchment: SH1 (Pillhill Brook), SH2 (River Avon), SH3 (River Wylye), and SH4 (River Avon). Curves show similar age distributions across sites, consistent with a common provenance dominated by Mesoproterozoic and Palaeoproterozoic sources.

Apatite U–Pb

On a Tera-Wasserburg plot, apatite U–Pb data frequently define one or more mixing lines, typically between a time-important radiogenic lead component and an initial common lead (Pb_c) component(s). The position of analyses along such arrays reflects the relative proportion of initial to radiogenic $^{207}Pb/^{206}Pb$ ratios (=F^{207}%), while lower intercepts indicate the timing of radiogenic Pb accumulation. Two hundred and fifty apatite U–Pb analyses were obtained across four samples (Table 1) (Supplementary Data 2).

Unanchored regressions through apatite analyses from each sample yield discordia with lower intercepts equivalent to late Cretaceous to

Paleogene ages and ordinate $^{207}Pb/^{206}Pb_i$ intercepts of ca. 0.8462, consistent with the Stacey and Kramers[48] model of terrestrial Pb_i evolution for late Cretaceous (ca. 65 Ma) crust. A free-fitted discordia line[49] through all analyses yields a lower intercept on concordia equivalent to 60 ± 3 Ma [mean square weighted deviation = 341, $p(\chi^2) = 0$] and an upper intercept $^{207}Pb/^{206}Pb_i$ of 0.8462 ± 0.0023 (Fig. 3), interpreted to indicate the average time of radiogenic-Pb accumulation and the dominant common Pb signature, respectively.

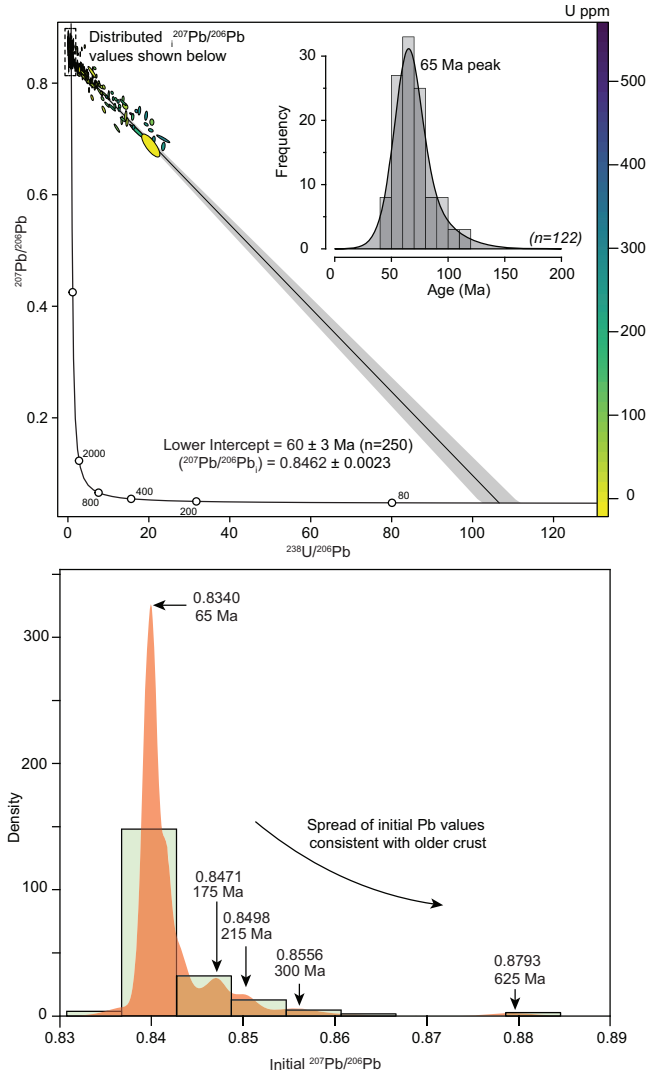

Fig. 3 | U–Pb isotopic data and Pb composition for detrital apatite grains from Salisbury Plain. *Top panel:* Tera-Wasserburg diagram for apatite analyses, coloured by U concentration (ppm). Error ellipses and intercept uncertainties are shown at 2σ. The regression is a least-squares best fit through the measured ratios alone and reflects more than one age component; nonetheless, radiogenic-Pb is dominated by a 60 Ma signal. (model-2 from IsoplotR[49]) with the grey band depicting the 2σ uncertainty envelope of the regression. The inset shows a kernel density estimate of ^{207}Pb-corrected ages for grains with relatively low common Pb content ($n = 122$) [$F^{207}Pb < 98\%$], indicating a peak at 65 Ma. *Bottom panel:* A kernel density estimation of initial common Pb compositions[48] for the detrital apatite population. A spread towards more radiogenic compositions (e.g. >0.85) indicates the incorporation of older common Pb components.

Additionally, individual ^{207}Pb corrected ages for each analyses were calculated using the Stacey and Kramers[48] terrestrial Pb isotopic evolution model, with iteration until convergence. A kernel density estimate of these ^{207}Pb-corrected single-spot apatite ages with $F^{207}\%$ <98% ($n = 122$) yields a peak age of 65 Ma, overlapping within uncertainty with the regression lower intercept age (Fig. 3).

Despite being dominated by a ca. 65 Ma age component, the single-spot $^{207}Pb/^{206}Pb_i$ values, for detrital apatite, imply the presence of some older (>65 Ma) Pb relative to the Stacey and Kramers[48] model. A kernel density estimate of apparent Pb model ages hints at older apatite components (175, 215, 300 and 625 Ma), but no radiogenic age can be calculated for these as they are dominated by common Pb (Fig. 3).

Apatite morphology

Apatite grains are anhedral to subhedral, with rounded shapes suggesting mechanical abrasion during sediment transport (Fig. 4). Imaging reveals homogeneous internal textures with low-intensity CL response. The absence of clear zoning or relic magmatic textures suggests limited thermal overprinting, typical of authigenic sedimentary or low-temperature diagenetic apatite. The consistent CL response and morphology across multiple grains (e.g. SH4.3, SH3.41) imply a detrital population sourced from mature, potentially chemically weathered sedimentary source material (Fig. 4).

Discussion

Kolmogorov–Smirnov tests of zircon age spectra from each river sand sample indicate no statistically significant differences, indicating the zircon age cargo of all samples is indistinguishable and remarkably uniform. This inter-sample consistency supports the aggregation of all concordant U–Pb zircon dates ($n = 401$) into a composite dataset for interpretation (Fig. 2). Moreover, the consistency of detrital zircon signatures between samples provides a robust regional detrital fingerprint signal for Salisbury Plain, rather than any sample-specific anomalies.

The compiled age spectrum spans 3396–285 Ma (Fig. 2) and is dominated by Meso to Paleoproterozoic peaks at ca. 1090, 1690, and 1740 Ma, consistent with an ultimate provenance from specific tectonostratigraphic domains of Laurentian basement from northern Britain (Fig. 1), including the Grenville, Penokean, and Trans-Hudson orogens[50–52].

Such Mesoproterozoic age modes are conspicuously absent in the Gondwanan-derived crystalline basement of southern Britain[53]. Instead, East Avalonian and Megumian age modes dominate the bedrock of Wales and southern England (Fig. 1) and include rocks from the Cadomian orogeny (ca. 650–600 Ma)[54,55], Neoproterozoic arc-related magmatism (590–540 Ma)[56], Silurian–Devonian intrusions (ca. 430–390 Ma)[53], Carboniferous (370–360 Ma)[57] and Variscan metamorphic overprinting and granite emplacement (~300 Ma)[58]. Such non-Laurentian ages would be diagnostic markers for distinguishing local, first-cycle basement contributions to the detrital budget of Salisbury Plain. If Salisbury Plain detritus had been introduced by glacial transport, the ice-flow directions most relevant to detrital zircon fingerprint would have been southward from the English Midlands or south-westward from Wales[38,59]. However, the dearth of East Avalonian and Megumian ages (only 8% of zircon are Phanerozoic) (Fig. 2) and the uniformity of age spectra across multiple catchments, coupled with

Table 1 | A summary table of sample localities and the underlying geology

Sample	Latitude	Longitude	UTM	River	Underlying geology
SH1	51.19809	−1.55350	30U 601065E, 5672848 N	Pillhill Brook	Seaford Chalk Formation
SH2	51.17070	−1.78518	30U 584928E, 5669510 N	Avon	Seaford Chalk Formation
SH3	51.15671	−2.06805	30U 565173E, 5667665 N	Wylye	West Melbury Marly Chalk Formation
SH4	51.05465	−1.77801	30U 585644E, 5656613 N	Avon	Newhaven Chalk Formation

Fig. 4 | Cathodoluminescence images of zircon and apatite grains with laser ablation spots. The top three rows show zircon grain images with sample identifiers, the calculated concordia age, and their respective 2σ uncertainties. Images of apatite are shown in the bottom two rows with ^{207}Pb-corrected ages with 2σ uncertainties annotated.

the scarcity of local bedrock sources, demonstrates that the detrital zircon assemblage is not first-cycle material locally derived or transported from the underlying East Avalonian and Megumian basement terranes (Fig. 5).

Our results are consistent with the maximum southern extent of known ice-flow vectors for Pleistocene glaciations[38,59,60]. During the Anglian Stage, the most intense recent glaciation, ice margins are generally interpreted to be to the north of Salisbury Plain[38]. Furthermore, there is no unequivocal evidence that ice penetrated onto the plateau as the Salisbury Plain lacks undisputed tills, erratics, or other diagnostic indicators of glacial activity[61–63] that could evidence long-distance erratic transport or outwash of

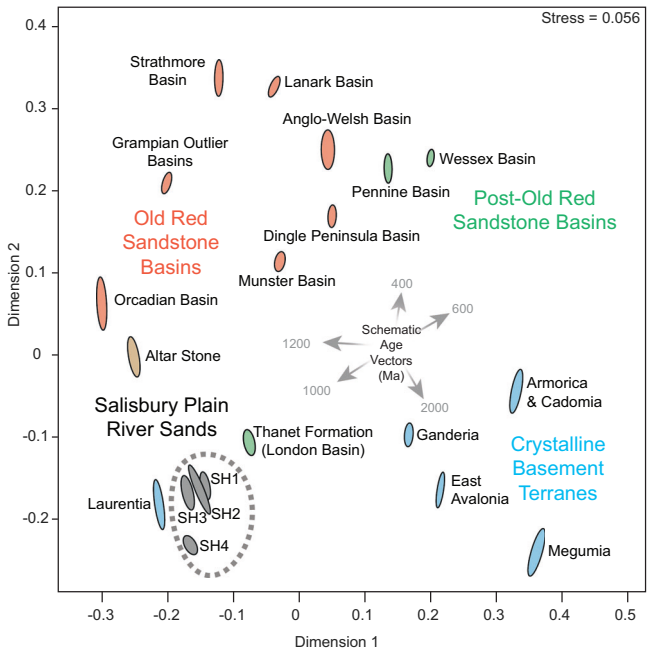

Fig. 5 | A multidimensional scaling plot of concordant zircon ages from stream sediment samples (SH1–SH4) and comparative age datasets, including crystalline source terranes and sedimentary basins. Schematic age mode vectors illustrate how discrete ages influence the positioning of individual datasets. Sources are provided in the methods section. Uncertainty ellipses are shown at 2σ uncertainty[97]. Stress values quantify how well the plot distances represent the original dataset's dissimilarities. Values below 0.15 indicate an 'excellent' fit[97].

material from northern Britain. Even if glacial erratics and meltwater outwash had contributed minor volumes of sediment, the local Chalk is nearly devoid of zircon; therefore, any extraneous zircon input would strongly influence the river sand detrital zircon signature.

Ultimately, the detrital zircon cargo of Salisbury Plain necessitates a north-to-south sediment transport and recycling mechanism from northern Britain other than glacial transport. To investigate potential sediment sources, we compare the age spectra of Salisbury Plain zircon population with detrital datasets from Paleogene, Carboniferous, and Devonian sedimentary units across Britain and Ireland (Fig. 5).

Of relevance here is the Thanet Formation, a ca. 30 m thick early Palaeocene (59.2−56 Ma) fine-grained glauconitic sand unit deposited in shallow marine conditions within the London Basin[64,65], which contains a detrital zircon age cargo statistically indistinguishable from the Salisbury Plain dataset (KS test, $P > 0.05$; Fig. 5)[13]. The Thanet Formation sits unconformably atop the Chalk Groups of Salisbury Plain[28] (Fig. 1), suggesting that these rocks or related London Basin strata served as an intermediary source of Laurentian zircon now incorporated into modern river sands of Salisbury Plain (Fig. 1).

More broadly, the Thanet Formation should be considered within the context of the wider Paleogene succession that formerly covered much of Salisbury Plain (Fig. 1). This cover includes floodplain, estuarine, marginal-marine, and marine deposits preserved today in the Hampshire and London Basins, as well as in remnant form as the Clay-with-Flints deposits[30,66]. Such Palaeogene deposits would have mantled the Salisbury Plain Chalk (Fig. 1) prior to their removal during Neogene erosion, and served as the host for the sarsen silcretes of the Marlborough Downs and Stonehenge landscape[67]. Their erosion and recycling during Paleogene basin inversion provides a plausible pathway for the release of refractory heavy minerals into the zircon-poor Salisbury Plain, consistent with the detrital signature (Fig. 2). In this context, the Thanet Formation represents a component of a larger Paleogene cover sequence that collectively functioned as a local reservoir for recycled Laurentian zircon.

Alternatively, it remains possible that zircon is present in trace quantities within Salisbury Plain Chalk (Fig. 1) and that the Thanet Formation and Chalk record sediment derivation from a broadly similar drainage network. In this case, the Thanet Formation would represent a related, rather than uniquely required, source-to-sink intermediary. In any case, the close similarity between the Thanet and Salisbury Plain zircon age spectra (Fig. 5) supports the interpretation that Paleogene strata acted as the principal recycled source for zircon within modern stream sand on Salisbury Plain.

We posit that during Alpine Orogen uplift and subsequent denudation of the London Basin[68,69], the overlying Thanet Formation released its detrital cargo of refractory minerals onto the zircon-poor Chalk Groups of southern Britain (Fig. 1). Indeed, several kilometres of London Basin strata may have been removed during the Paleogene to Eocene[66,70], resulting in a lag of durable heavy minerals that were later reworked into modern stream sediments. Although much of the Cenozoic overburden on Salisbury Plain has been removed, Laurentian zircons could have persisted in remnant Palaeogene sands, accumulating and concentrating in local topographic lows and along palaeodrainage channels, such as the ancestral courses of the Avon and Wylye rivers (Fig. 1). A combination of remnant sediment and ancient fluvial pathways provides a plausible mechanism for zircon survival on Salisbury Plain despite extensive erosion.

How fine-grained Laurentian detritus became incorporated into the Thanet Formation remains uncertain[13]. While the reworking of ORS is one possible pathway, the relative scarcity of Grampian and Laurentian-aged zircon in the Thanet Formations suggests that this mechanism cannot have been the sole contributor. Rather, a mixture of recycled sources, including Pennine Basin rocks and ORS, likely fed the London Basin during the Paleogene uplift of the Wales–Brabant Massif[13]. Alternatively, longshore drift along the Palaeocene proto-North Sea margin transported northern detritus to the Thanet Formation, which was subsequently mixed via the proto-Thames River[71]. Ultimately, the Laurentian zircon fingerprint (Fig. 2) of Salisbury Plain stream sediment reflects polycyclic sediment routing pathways in Britain dominated by the reworking of earlier strata and does not support direct delivery via glacial transport.

The detrital fingerprint of Salisbury Plain also helps inform hypotheses regarding Mynydd Preseli bluestone ice transport from west Wales (Fig. 1). Rhyolite Bluestones from the Stonehenge area and the Mynydd Preseli have been dated to the Darriwilian (464–462 Ma), consistent with a source from the Fishguard Volcanic Group[25]. From 550 U–Pb analyses in our study, a single concordant analysis at 464 ± 16 Ma from SH3 (River Wylye) represents the only potential Bluestone-derived zircon (Fig. 2 and Supplementary Data 1). Such isolated, outlier zircon are a feature of large *n* detrital datasets, reflecting the extreme durability and long multi-cycle residence times of zircon. Moreover, Darriwilian zircon are not unique to the Mynydd Preseli. Comparable ages occur sporadically in recycled Cenozoic sedimentary units across southern Britain, including the Thanet Formation[13]. Thus, the most parsimonious explanation for this lone 464 Ma grain is its incorporation through multi-cycle sedimentary recycling from Cenozoic units, rather than the arrival of any sediment derived from the Mynydd Preseli.

If the bluestones are glacial erratics, then the ca. 464 Ma detrital age would be expected to be much more common throughout the drainage systems on Salisbury Plain. It is not; hence, this observation is consistent with previous studies, which do not report bluestone clasts in Salisbury Plain stream sediments[37,63]. Moreover, the river sands contain no coarse-grained first-cycle lithic clasts (e.g. granite, gneiss, or mafic fragments) that would be expected if Laurentian zircon had arrived as primary erratic detritus. Combined with the well-rounded, compositionally mature nature of the zircon-bearing sands (Fig. 4 and Supplementary Data 3), this indicates a history of multi-cycle sedimentary recycling rather than direct glacial transport.

Salisbury Plain is dominated by the White Chalk Subgroup, which was deposited in a stable epicontinental shelf setting throughout the mid-to-late Cretaceous[30]. Specifically, the river sand samples are underlain by the Seaford (SH1, SH2), West Melbury (SH3) and Newhaven (SH4) Chalk formations, which span the Cenomanian to Santonian stages of the mid-

Cretaceous (Fig. 1)[28,30]. Phosphatic horizons are well documented in these rocks, especially in the Seaford Chalk near Stonehenge, where thick, lenticular phosphatic deposits occur within fault-controlled submarine channels[42]. These phosphatic Chalk horizons, spanning the Late Cretaceous, are rich in phosphatised faecal pellets from benthonic detritus feeders, along with minor phosphatised foraminifera and fish remains, providing a plausible local source of bioapatite that was subsequently reworked into modern stream sediments[42,43] (Fig. 1) (Supplementary Data 3).

Detrital apatite U–Pb analyses from Salisbury Plain River sands yield a dominant array on a Tera-Wasserburg plot, implying most radiogenic-Pb retention at 60 ± 3 Ma ($n = 250$). Alternatively, ^{207}Pb corrected ages for apatite, with an $F^{207} < 98\%$ span 115–32 Ma, with a dominant age peak at ~65 Ma (Fig. 3). Palaeogene U–Pb apatite ages postdate the youngest Chalk formations in Britain, including the Portsdown Chalk (Fig. 1) (ca. 77–70 Ma[30]). Therefore, we interpret the ca. 60 Ma date to reflect post-depositional U–Pb disturbance of a heterogeneous Mesozoic population, dominated by bioapatite[42,43]. Bioapatite is consistent with the Chalk formations underlying the study area being deposited in shallow marine environments conducive to biogenic phosphate accumulation[42,43,72].

The scattering of $^{207}Pb/^{206}Pb_i$ ratios up to 0.8793 hints towards the presence of older primary apatite. These elevated $^{207}Pb/^{206}Pb_i$ ratios exceed expected ratios for ca. 60 Ma crustal Pb compositions, as modelled by Stacey and Kramers[48], implying prolonged U–Pb evolution in some apatite before ca. 60 Ma and thus minor inheritance from other older sources. The preservation of variable $^{207}Pb/^{206}Pb_i$ values, coupled with a coherent lower intercept age, reflects the contrasting chemical mobility of U and Pb in apatite[73,74] during a period of fluid flux at approximately 60 Ma (Fig. 3).

Apatite grains from Salisbury Plain typically occur as 400–100 µm euhedral to anhedral, angular fragments exhibiting faint sector zonation, with up to 500 ppm of U (Fig. 4). The porous, poorly crystalline structure of bioapatite facilitates U gain (due to the solubility of U^6) from oxidised seawater and pore fluids[75,76]. In contrast, Pb^{2+} is relatively immobile and structurally bound or sequestered within lattice defects[75]. As a result, recrystallisation of U-rich apatite during post-depositional alteration dominates the lower-intercept age, whereas $^{207}Pb/^{206}Pb_i$ ratios in low-U apatite grains (or domains) are better preserved and retain evidence of older, heterogeneous detrital components (Fig. 3).

Authigenic marine phosphates typically exhibit extremely low Th/U ratios, leading to highly elevated $^{206}Pb/^{208}Pb$ ratios in authigenic apatite[76,77], due to bacterial scavenging of U from seawater, which has negligible thorium[75,76]. However, Salisbury Plain apatite displays relatively low $^{206}Pb/^{208}Pb$ ratios (median ~0.59, with no anomalously high values) despite high uranium concentrations (median ~34 ppm, with some grains exceeding 500 ppm), suggesting Salisbury Plain apatite grains are unlikely to be pristine primary marine authigenic phosphates with low Th/U ratios. Instead, the comparatively low $^{206}Pb/^{208}Pb$ ratios, combined with elevated U, suggest that diagenetic recrystallisation or modification processes introduced additional Th and common Pb into apatite, thereby diluting the radiogenic Pb signature of apatite[76,77]. These processes are consistent with endemic bioapatite from phosphatic Chalks, which have undergone partial recrystallisation during Paleogene tectonically driven fluid alteration.

At ca. 60 Ma, the nascent Alpine Orogeny[69,78] initiated far-field compressional stresses across western Europe, driving prolonged basin inversion in southern Britain. This tectonism resulted in the folding of the Chalk at Lulworth Cove and the reactivation of structures associated with the broader Purbeck–Isle of Wight Disturbance[79]. Indeed, phosphatic horizons occur in lenticular, channelised bodies controlled by local compressional faulting on Salisbury Plain[42]. Thus, it is feasible that fluid-rock interaction at this time, facilitated by inversion-related deformation and faulting, enabled Pb mobilisation and recrystallisation within detrital (bio)apatite[75,76].

The apparent absence of Laurentian apatite in the modern river sediments of Salisbury Plain, despite the presence of Laurentian-derived zircon, likely reflects the different susceptibility of both minerals to destruction during sedimentary processes. Apatite is more liable to chemical dissolution and alteration during sedimentary reworking, whereas zircon is highly durable[8,80,81]. Consequently, the survival of multi-cyclic Laurentian zircon without corresponding apatite is consistent with the selective removal of apatite during chemical weathering and sedimentary recycling. Such a decoupled zircon-apatite fingerprint for Salisbury Plain is inconsistent with first-cycle glacially-derived detritus, which would necessarily deliver zircon and apatite from crystalline sources.

Conclusions

New U–Pb dates for detrital zircon and apatite collected from streams draining Salisbury Plain, England, reveal Cenozoic sediment transport and reworking, which help inform hypotheses on the transport of the megaliths at Stonehenge.

Zircon dates span 3396–285 Ma, with prominent age peaks at 1089, 1690, and 1740 Ma, consistent with derivation from the Laurentian crystalline basement to the north. However, Quaternary glacial reconstructions indicate that ice sheets did not extend as far south as Salisbury Plain, making direct transport of zircon-bearing erratics or glacial outwash unlikely. Moreover, the multi-cycle nature of detrital zircon, combined with the absence of proximal crystalline sources from East Avalonian or Megumian basement rocks, argues against a primary glacial origin from southwest Wales or the English Midlands. Indeed, among the 550 detrital zircon analyses, only a single concordant grain from Salisbury Plain stream sediments yields an age (464 ± 16 Ma) consistent with the characteristic Darriwilian ages of the Mynydd Preseli bluestones of southwest Wales. The extreme rarity of this signature underscores the negligible contribution of southwest Welsh, or specifically Preseli, crystalline rock input to the detrital cargo of Salisbury Plain. If ice of sufficient thickness and extent had transported tens of large, multi-tonne bluestone erratics from west Wales to Salisbury Plain, it would be expected to leave a pronounced Darriwilian zircon signature in the fine detrital fraction; its near absence instead indicates that such large-scale glacial transport did not occur.

The Palaeocene Thanet Formation of the London Basin, which unconformably overlies the Chalk of Salisbury Plain, possesses a zircon age spectrum statistically indistinguishable from that of modern stream sands, representing a more plausible source of the stream zircon detritus. Laurentian zircon was recycled through Paleogene sedimentary rocks and remobilised during ongoing denudation in southern Britain, providing a sustained and local reservoir of reworked material.

Detrital apatite is dominated by a ca. 60 Ma population, consistent with recrystallised bioapatite derived from local Late Cretaceous Chalk phosphatic horizons of Salisbury Plain. These apatites have high uranium concentrations (median ~34 ppm, with some grains exceeding 500 ppm) but relatively low $^{206}Pb/^{208}Pb$ ratios (~0.59), reflecting diagenetic recrystallisation and the partial introduction of common Pb and thorium. Variously radiogenic $^{207}Pb/^{206}Pb_i$ compositions suggest a minor, heterogeneous Mesozoic component. We interpret this as a mixture of bioapatite and recrystallised phosphate, partially reset during early Paleogene fluid flow linked to basin inversion and Alpine Orogeny-related compressional stresses.

Ultimately, the detrital zircon and apatite records from Salisbury Plain capture the imprint of early Paleogene tectonism linked to the nascent Alpine Orogeny. Reworking of the Thanet Formation and the Chalk during basin inversion released recycled Laurentian zircon onto Salisbury Plain, while coeval fluid–rock interaction reset U–Pb systematics in locally derived bioapatite. These minerals archive complementary mechanical and chemical responses to Paleogene crustal deformation, revealing a unified signal of Alpine-induced sedimentary remobilisation in southern Britain. This tectonically driven reworking provides a parsimonious alternative to sediment transport via glaciation, explaining the presence of far-travelled fine detritus that characterises the detrital mineral spectrum of Salisbury Plain. Consequently, we consider direct glacial transport of Stonehenge's megaliths to the site's environs improbable.

Methods

Mineral separation

Four river sand samples (SH1–SH4) weighing ca. 1 kg were collected from Salisbury Plain (Fig. 1) (Table 1). The collected material was processed at the John de Laeter Centre, Curtin University. Unprocessed sand was first sieved at ≤250 µm to yield ca. 100 g fractions, which subsequently underwent heavy mineral separation using a Jasper Canyon Research shaking platform[82]. Coarse magnetic minerals were removed using a handheld neodymium magnet. To further fractionate the fine fraction, lithium heteropolytungstate heavy liquid (2.85 g cm^{-3}) was used to remove light minerals (e.g. quartz, feldspars). A round of Frantz isodynamic magnetic separation (using a side-slope angle of 10° and an Amperage of 1.7) allowed for the retrieval of a final non-magnetic, heavy mineral concentrate. Lastly, the non-magnetic fraction (≤0.2 g) was bulk mounted into 25 mm diameter epoxy discs.

Mounts were polished to a one µm finish, and embedded minerals were imaged using a TESCAN Integrated Mineral Analyser in the John de Laeter Centre, Curtin University, with a 1 µm resolution for back-scattered electron imaging, and 9 µm resolution for energy dispersive X-ray spectroscopy dot mapping. Additional imaging was performed using a Clara FE-SEM to identify internal textures and crystal morphologies, which aided in the selection of laser ablation sites.

Zircon U–Pb analysis

Analyses were performed using the LA-ICP-MS instrumentation at the GeoHistory Facility, John de Laeter Centre, Curtin University (Supplementary Data 1). Zircon U–Pb data were collected using an Agilent 8900 ICP-MS. Ablations from zircon grains were created using a RESOlution LR193 nm ArF equipped with a Laurin Technic S-155 cell. The carrier gas was high-purity argon with a flow rate of 0.98 L min^{-1}. A spot size of 28 µm was combined with an on-sample fluence of ~2.8 J cm^{-2} and a repetition rate of 5 Hz. Two cleaning pulses preceded each analysis, and signals from zircon and the background were analysed for 30 s. The sample cell was cleaned using ultrahigh-purity He (350 ml min^{-1}) and N_2 (3.8 ml min^{-1}). The dwell times for U–Pb measurements were as follows: 0.1 s for ^{238}U and ^{232}Th, 0.2 s for ^{208}Pb, 0.7 s for ^{207}Pb, 0.4 s for ^{206}Pb, and 0.3 s for ^{204}Pb and ^{202}Hg.

GJ1 zircon 601.95 ± 0.40 Ma[83,84] was the primary reference material for all zircon U–Pb analyses. Secondary reference zircons were analysed after every ~15 unknowns and included Plešovice = 337.13 ± 0.37 Ma[85]; OG1 = 3465.4 ± 0.6 Ma[86] and Maniitsoq = 3008.70 ± 0.72 Ma[87]. Calculated weighted mean U–Pb and Pb-Pb dates for secondary reference zircon were within 2σ uncertainty of published values (Supplementary Data 1).

We measure U–Pb discordance using concordia log distance (%) and apply a ±10% threshold to define discordance. Over 95% of analyses within our discordance filter are within analytical uncertainty of concordia at the 2SE confidence level. We use single-spot concordia ages for further statistical analysis, which offers several advantages over single-ratio U–Pb or Pb–Pb ages[26].

Apatite U–Pb analysis

In-situ apatite U–Pb analyses were conducted using a Nu Plasma II multi-collector mass spectrometer coupled to a Resonetics S-155-LR 193 nm excimer laser ablation system at the GeoHistory Facility, John de Laeter Centre, Curtin University. Apatite grains were ablated with the same laser system as zircon, but used a beam diameter of 38 µm (Supplementary Data 2).

The following masses were measured: ^{202}Hg, $^{204}(Pb + Hg)$, ^{206}Pb, ^{207}Pb, ^{208}Pb, and ^{238}U. All masses were measured on ion counters for 210 cycles with an integration time of 0.3 s. The laser fluence measured at the sample surface was ca. 3.5 J cm^{-2}, and a pulse frequency of 5 Hz was used. Data acquisition consisted of two cleaning pulses, a 40–20 s blank flush out, a 15–30 s ablation time, and a total of 45 s of baseline acquisition. The sample cell was flushed with ultrahigh-purity He (320 ml min^{-1}) and N_2 (1.2 ml min^{-1}), and ultra-high-purity Ar was employed as the plasma carrier gas.

Comparative datasets

Zircon U–Pb data for the crystalline basement rocks of Britain, Ireland and continental Europe were sourced from refs. 13,88. Detrital zircon datasets from Britain used for comparison include Orcadian Basin ORS[52], Grampian Outlier ORS[89], Strathmore Basin (northern Midland Valley)[90], Lanark Basin (southern Midland Valley)[91], Pennine Basin[14,18,92,93], Anglo-Welsh Basin ORS[14], Wessex Basin[15], and the Thanet Formation, London Basin[13]. For Ireland, detrital datasets include the Dingle Peninsula Basin ORS[88] and Munster Basin ORS[44]. Age data for the Altar Stone were sourced from refs. 26,94. All zircon U–Pb data for sedimentary and crystalline rocks within Britain and Ireland were filtered for discordance.

Two-sample, two-sided Kolmogorov–Smirnov (KS) tests were used to compare the detrital zircon age spectra of Salisbury Plain stream sand samples with compiled zircon datasets. This test assesses the maximum difference between the cumulative density functions of the two distributions, evaluating the null hypothesis that both spectra are drawn from the same underlying population. The significance of the result is determined by a critical value that depends on the sample sizes and the chosen confidence level.

Reporting summary

Further information on research design is available in the Nature Portfolio Reporting Summary linked to this article.

Data availability

All data used in this manuscript are included in the published article (and its supplementary data files). All data has been uploaded to FigShare[95] at https://figshare.com/s/d12a61a54f5647d60a53. Supplementary data files contain all isotopic and automated mineralogy data used to generate the figures.

Received: 11 August 2025; Accepted: 5 December 2025;
Published online: 21 January 2026

References

1. Morón, S. et al. Long-lived transcontinental sediment transport pathways of East Gondwana. *Geology* **47**, 513–516 (2019).
2. Dröllner, M., Barham, M. & Kirkland, C. L. Reorganization of continent-scale sediment routing based on detrital zircon and rutile multi-proxy analysis. *Basin Res.* **35**, 363–386 (2023).
3. Cawood, P. A., Hawkesworth, C. J. & Dhuime, B. Detrital zircon record and tectonic setting. *Geology* **40**, 875–878 (2012).
4. Gehrels, G. & Pecha, M. Detrital zircon U-Pb geochronology and Hf isotope geochemistry of Paleozoic and Triassic passive margin strata of western North America. *Geosphere* **10**, 49–65 (2014).
5. Moecher, D. P. & Samson, S. D. Differential zircon fertility of source terranes and natural bias in the detrital zircon record: implications for sedimentary provenance analysis. *Earth Planet. Sci. Lett.* **247**, 252–266 (2006).
6. Andersen, T. Age, Hf isotope and trace element signatures of detrital zircons in the Mesoproterozoic Eriksfjord sandstone, southern Greenland: are detrital zircons reliable guides to sedimentary provenance and timing of deposition? *Geol. Mag.* **150**, 426–440 (2012).
7. Salama, W., Anand, R. R., Tunmer, W. & Aspandiar, M. Regolith characterization and landscape evolution for geochemical exploration of the covered Yamarna Terrane, Western Australia. *J. Geochem. Explor.* **232**, 106881 (2022).
8. Clarke, A. J. I., Kirkland, C. L., Glorie, S., Quentin de Gromard, R. & Tucker, N. M. Detrital zircon and apatite reveal Paleoproterozoic rifting along the eastern margin of the Yilgarn Craton. *Precambrian Res.* **414**, 107602 (2024).
9. Bonich, M. B., Samson, S. D. & Fedo, C. M. Incongruity of detrital zircon ages of granitic bedrock and its derived alluvium: an example from the Stepladder Mountains, southeastern California. *J. Geol.* **125**, 337–350 (2017).

10. Zametzer, A. et al. When the river meets the sea: transport and provenance in a long-lived estuary. *Basin Res.* **36**, e70001 (2024).
11. Morton, A. C. & Hallsworth, C. Identifying provenance-specific features of detrital heavy mineral assemblages in sandstones. *Sediment. Geol.* **90**, 241–256 (1994).
12. Dröllner, M., Barham, M., Kirkland, C. L., Zametzer, A. & Schulz, M. Australian continental-scale heavy mineral patterns track climate, weathering and erosion. *Sedimentology* https://doi.org/10.1111/sed.70008 (2025).
13. Stevens, T. & Baykal, Y. Detrital zircon U-Pb ages and source of the late Palaeocene Thanet Formation, Kent, SE England. *Proc. Geol. Assoc.* **132**, 240–248 (2021).
14. Morton, A., Waters, C., Fanning, M., Chisholm, I. & Brettle, M. Origin of Carboniferous sandstones fringing the northern margin of the Wales-Brabant Massif: insights from detrital zircon ages. *Geol. J.* **50**, 553–574 (2015).
15. Morton, A., Knox, R. & Frei, D. Heavy mineral and zircon age constraints on provenance of the Sherwood Sandstone Group (Triassic) in the eastern Wessex Basin, UK. *Proc. Geol. Assoc.* **127**, 514–526 (2016).
16. Clarke, A. J., Kirkland, C. L. & Glorie, S. A day at the beach: a portrait of British geology through sand. *J. Geol. Soc.* **182**, jgs2025–jgs2043 (2025).
17. Barham, M. et al. Sediment routing and basin evolution in Proterozoic to Mesozoic east Gondwana: a case study from southern Australia. *Gondwana Res.* **58**, 122–140 (2018).
18. Morton, A. C., Chisholm, J. I. & Frei, D. Provenance response to evolving palaeogeography recorded by Carboniferous sandstones in the northern Pennine Basin, UK. *Sediment. Geol.* **470**, 106691 (2024).
19. Kelloway, S. J. et al. Sourcing olive jars using U-Pb ages of detrital zircons: a study of 16th century olive jars recovered from the Solomon Islands. *Geoarchaeology* **29**, 47–60 (2014).
20. Tochilin, C. et al. Sourcing temper sands in ancient ceramics with U–Pb ages of detrital zircons: a southwest Pacific test case. *J. Archaeol. Sci.* **39**, 2583–2591 (2012).
21. Pitts, M. *How to Build Stonehenge* (Thames & Hudson, 2022).
22. Nash, D. J. et al. Origins of the sarsen megaliths at Stonehenge. *Sci. Adv.* **6**, https://doi.org/10.1126/sciadv.abc0133 (2020).
23. Ciborowski, T. J. R. et al. Local and exotic sources of sarsen debitage at Stonehenge revealed by geochemical provenancing. *J. Archaeol. Sci.***53**, 104406 (2024).
24. Ixer, R. & Bevins, R. The bluestones of Stonehenge. *Geol. Today* **33**, 180–184 (2017).
25. Bevins, R., Atkinson, N., Ixer, R. & Evans, J. U–Pb zircon age constraints for the Ordovician Fishguard Volcanic Group and further evidence for the provenance of the Stonehenge bluestones. *J. Geol. Soc.* **174**, 14–17 (2016).
26. Clarke, A. J. I. et al. A Scottish provenance for the Altar Stone of Stonehenge. *Nature* **632**, 570–575 (2024).
27. Ixer, R., Bevins, R., Pirrie, D., Turner, P. & Power, M. No provenance is better than wrong provenance: Milford Haven and the Stonehenge sandstones. *Wilts. Archaeol. Nat. Hist. Mag.* **113**, 1–15 (2020).
28. Bristow, R., Mortimore, R. & Wood, C. Lithostratigraphy for mapping the Chalk of southern England. *Proc. Geol. Assoc.* **108**, 293–315 (1997).
29. Allen, D. & Crane, E. *The chalk aquifer of the Wessex Basin* (British Geological Survey, 2019).
30. Hopson, P. *A stratigraphical framework for the Upper Cretaceous Chalk of England and Scotland with statements on the Chalk of Northern Ireland and the UK Offshore Sector* (British Geological Survey, 2005).
31. Blackwood, J. & Tubbs, C. A quantitative survey of chalk grassland in England. *Biol. Conserv.* **3**, 1–5 (1970).
32. Parker Pearson, M. et al. Craig Rhos-y-felin: a Welsh bluestone megalith quarry for Stonehenge. *Antiquity* **89**, 1331–1352 (2015).
33. Parker Pearson, M. et al. Stonehenge and its altar stone: the significance of distant stone sources. *Archaeol. Int.* **27**, 113–137 (2024).
34. John, B. S. A bluestone boulder at Stonehenge: implications for the glacial transport theory. *EG Quat. Sci. J.* **73**, 117–134 (2024).
35. Thorpe, R. S. et al. The geological sources and transport of the bluestones of stonehenge, Wiltshire, UK. *Proc. Prehist. Soc.* **57**, 103–157 (1991).
36. John, B. *The Stonehenge Bluestones* (Greencroft Books, 2018).
37. Scourse, J. In *Proceedings of the British Academy* 271–314 (Oxford University Press, 1905).
38. Gibbard, P. L. & Clark, C. D. in *Developments in Quaternary Sciences* Vol. 15 (eds Jürgen Ehlers, Philip L. Gibbard, & Philip D. Hughes) 75–93 (Elsevier, 2011).
39. Veness, R. L. et al. Modelling erratic dispersal accounting for shifting ice flow geometries: a new method and explanations of erratic dispersal of the British–Irish Ice Sheet. *J. Quat. Sci*. https://doi.org/10.1002/jqs.3720 (2025).
40. Hagg, W. *Glaciology and Glacial Geomorphology* 151–165 (Springer Berlin Heidelberg, 2022).
41. Eyles, N. The role of meltwater in glacial processes. *Sediment. Geol.* **190**, 257–268 (2006).
42. Mortimore, R. N. et al. Stonehenge—a unique Late Cretaceous phosphatic Chalk geology: implications for sea-level, climate and tectonics and impact on engineering and archaeology. *Proc. Geol. Assoc.* **128**, 564–598 (2017).
43. Pacey, N. R. The mineralogy, geochemistry and origin of pelletal phosphates in the English Chalk. *Chem. Geol.* **48**, 243–256 (1985).
44. Fairey, B. J. et al. Sedimentary provenance of the Upper Devonian Old Red Sandstone of southern Ireland: an integrated multi-proxy detrital geochronology study. *J. Geol. Soc.* **181**, jgs2023–jgs2110 (2024).
45. Lancaster, P. J., Daly, J. S., Storey, C. D. & Morton, A. C. Interrogating the provenance of large river systems: multi-proxy in situ analyses in the Millstone Grit, Yorkshire. *J. Geol. Soc.* **174**, 75–87 (2017).
46. Zoleikhaei, Y., Mulder, J. A. & Cawood, P. A. Integrated detrital rutile and zircon provenance reveals multiple sources for Cambrian sandstones in North Gondwana. *Earth Sci. Rev.* **213**, 103462 (2021).
47. Gehrels, G. Detrital zircon U-Pb geochronology: current methods and new opportunities. *Tectonics of Sedimentary Basins: Recent Advances* 45–62 (Wiley-Blackwell, 2011).
48. Stacey, J. T. & Kramers, J. Approximation of terrestrial lead isotope evolution by a two-stage model. *Earth Planet. Sci. Lett.* **26**, 207–221 (1975).
49. Vermeesch, P. IsoplotR: A free and open toolbox for geochronology. *Geosci. Front.* **9**, 1479–1493 (2018).
50. Hoffman, P. F. Did the breakout of laurentia turn gondwanaland inside-out? *Science* **252**, 1409–1412 (1991).
51. Cawood, P. A., Nemchin, A. A., Strachan, R., Prave, T. & Krabbendam, M. Sedimentary basin and detrital zircon record along East Laurentia and Baltica during assembly and breakup of Rodinia. *J. Geol. Soc.* **164**, 257–275 (2007).
52. Strachan, R., Olierook, H. & Kirkland, C. Evidence from the U-Pb-Hf signatures of detrital zircons for a Baltican provenance for basal Old Red Sandstone successions, northern Scottish Caledonides. *J. Geol. Soc.* **178**, jgs2020–jgs2241 (2021).
53. Henderson, B. J., Collins, W. J., Murphy, J. B., Gutierrez-Alonso, G. & Hand, M. Gondwanan basement terranes of the Variscan–Appalachian orogen: Baltican, Saharan and West African hafnium isotopic fingerprints in Avalonia, Iberia and the Armorican Terranes. *Tectonophysics* **681**, 278–304 (2016).
54. Murphy, J. B., Pisarevsky, S. & Nance, R. D. Potential geodynamic relationships between the development of peripheral orogens along the northern margin of Gondwana and the amalgamation of West Gondwana. *Mineral. Petrol.* **107**, 635–650 (2013).

55. Accotto, C., Azor, A., Martínez Poyatos, D., Pedrera, A. & González Lodeiro, F. Reorganization of Northern Peri-Gondwanan Terranes at Cambrian–Ordovician Times: Insights from the Detrital Zircon Record of the Ossa-Morena Zone (SW Iberian Massif). *Lithosphere* **2022** https://doi.org/10.2113/2022/6187518 (2022).
56. Pharaoh, T. C. & Carney, J. N. *Introduction to the Precambrian Rocks of England and Wales* Vol. 1–18 (Joint Nature Conservation Committee-Chapman and Hall, 2000).
57. Stephenson, D., Loughlin, S.C., Millward, D., Waters, C. N. & Williamson, I. T. *Carboniferous and Permian Igneous Rocks of Great Britain North of the Variscan Front* Vol. 27 (Joint Nature Conservation Committee, 2003).
58. Neace, E. R., Nance, R. D., Murphy, J. B., Lancaster, P. J. & Shail, R. K. Zircon LA-ICPMS geochronology of the Cornubian Batholith, SW England. *Tectonophysics* **681**, 332–352 (2016).
59. Clark, C. D. et al. Growth and retreat of the last British–Irish Ice Sheet, 31 000 to 15 000 years ago: the BRITICE-CHRONO reconstruction. *Boreas* **51**, 699–758 (2022).
60. Ely, J. C. et al. Behavioural tendencies of the last British–Irish Ice Sheet revealed by data–model comparison. *J. Quat. Sci.* **39**, 839–871 (2024).
61. McOmish, D., Field, D. & Brown, G. *The Field Archaeology of the Salisbury Plain Training Area* (Liverpool University Press, 2002).
62. Bowen, H. & Smith, I. F. Sarsen stones in Wessex: the Society's first investigations in the evolution of the landscape project. *Antiqu. J.* **57**, 185–196 (1977).
63. Green, C. P. Pleistocene river gravels and the stonehenge problem. *Nature* **243**, 214–216 (1973).
64. Ellison, R., Knox, R. O. B., Jolley, D. & King, C. A revision of the lithostratigraphical classification of the early Palaeogene strata of the London Basin and East Anglia. *Proc. Geol. Assoc.* **105**, 187–197 (1994).
65. Morton, A. C. The provenance and diagenesis of Palaeogene sandstones of southeast England as indicated by heavy mineral analysis. *Proc. Geologists' Assoc.* **93**, 263–274 (1982).
66. Harding, P., Nash, D. J., Ciborowski, T. J. R., Maniatis, G. & Colman, K. Earliest movement of sarsen into the stonehenge landscape: new insights from geochemical and visibility analysis of the cuckoo stone and tor stone. *Proc. Prehist. Soc.* **90**, 229–251 (2024).
67. Nash, D. J. et al. Petrological and geochemical characterisation of the sarsen stones at Stonehenge. *PLoS ONE* **16**, e0254760 (2021).
68. Hawkes, P. W., Fraser, A. J. & Einchcomb, C. C. G. The tectono-stratigraphic development and exploration history of the Weald and Wessex basins, Southern England, UK. *Geol. Soc. Lond. Spec. Publ.* **133**, 39–65 (1998).
69. Angrand, P. & Mouthereau, F. Evolution of the Alpine orogenic belts in the Western Mediterranean region as resolved by the kinematics of the Europe-Africa diffuse plate boundary. *Bull. Soc. Géol. Fr.* **192** https://doi.org/10.1051/bsgf/2021031 (2021).
70. Lewis, C. L., Green, P. F., Carter, A. & Hurford, A. J. Elevated K/T palaeotemperatures throughout Nortwest England: three kilometres of Tertiary erosion? *Earth Planet. Sci. Lett.* **112**, 131–145 (1992).
71. Gibbard, P. L., Hughes, P. D. & Rolfe, C. J. New insights into the Quaternary evolution of the Bristol Channel, UK. *J. Quat. Sci.* **32**, 564–578 (2017).
72. Muscente, A. D., Hawkins, A. D. & Xiao, S. Fossil preservation through phosphatization and silicification in the Ediacaran Doushantuo Formation (South China): a comparative synthesis. *Palaeogeogr. Palaeoclimatol. Palaeoecol.* **434**, 46–62 (2015).
73. Chew, D. M. & Spikings, R. A. Apatite U-Pb thermochronology: a review. *Minerals* **11**, 1095 (2021).
74. Kirkland, C. et al. Apatite: a U-Pb thermochronometer or geochronometer? *Lithos* **318**, 143–157 (2018).
75. Cumberland, S. A., Douglas, G., Grice, K. & Moreau, J. W. Uranium mobility in organic matter-rich sediments: a review of geological and geochemical processes. *Earth Sci. Rev.* **159**, 160–185 (2016).
76. Wang, H. et al. Rare earth element enrichment process of bioapatite in deep-sea REY-rich sediments. *Chem. Geol.* **662**, 122252 (2024).
77. Wang, Z. et al. Lead isotopes and rare earth elements geochemistry of global phosphate rocks: Insights into depositional conditions and environmental tracing. *Chem. Geol.* **639**, 121715 (2023).
78. Rosenbaum, G. & Lister, G. S. The Western Alps from the Jurassic to Oligocene: spatio-temporal constraints and evolutionary reconstructions. *Earth Sci. Rev.* **69**, 281–306 (2005).
79. Underhill, J. R. & Stoneley, R. Introduction to the development, evolution and petroleum geology of the Wessex Basin. *Geol. Soc. Lond. Spec. Publ.* **133**, 1–18 (1998).
80. Glorie, S. et al. Detrital apatite Lu–Hf and U–Pb geochronology applied to the southwestern Siberian margin. *Terra Nova* **34**, 201–209 (2022).
81. O'Sullivan, G., Chew, D., Kenny, G., Henrichs, I. & Mulligan, D. The trace element composition of apatite and its application to detrital provenance studies. *Earth Sci. Rev.* **201**, 103044 (2020).
82. Dumitru, T. A. A new zircon concentrating table designed for geochronologists. In *AGU Fall Meeting Abstracts*. Vol. 2016, pp. V23A-2956 (2016).
83. Jackson, S. E., Pearson, N. J., Griffin, W. L. & Belousova, E. A. The application of laser ablation-inductively coupled plasma-mass spectrometry to in situ U–Pb zircon geochronology. *Chem. Geol.* **211**, 47–69 (2004).
84. Horstwood, M. S. A. et al. Community-derived standards for LA-ICP-MS U-(Th-)Pb geochronology – uncertainty propagation, age interpretation and data reporting. *Geostand. Geoanal. Res.* **40**, 311–332 (2016).
85. Sláma, J. et al. Plešovice zircon—a new natural reference material for U–Pb and Hf isotopic microanalysis. *Chem. Geol.* **249**, 1–35 (2008).
86. Stern, R. A., Bodorkos, S., Kamo, S. L., Hickman, A. H. & Corfu, F. Measurement of SIMS instrumental mass fractionation of Pb isotopes during zircon dating. *Geostand. Geoanal. Res.* **33**, 145–168 (2009).
87. Marsh, J., Jørgensen, T., Petrus, J., Hamilton, M. & Mole, D. U-Pb, trace element, and hafnium isotope composition of the Maniitsoq zircon: A potential new Archean zircon reference material. In *Twenty-ninth Annual Goldschmidt Conference* p. 2161 (2019).
88. Fairey, B. et al. The provenance of the Devonian Old Red Sandstone of the Dingle Peninsula, SW Ireland; the earliest record of Laurentian and peri-Gondwanan sediment mixing in Ireland. *J. Geol. Soc.* **175**, jgs2017–jgs2099 (2018).
89. McKellar, Z., Hartley, A. J., Macdonald, D. I. M., Morton, A. & Frei, D. Sedimentology and provenance of the Lower Old Red Sandstone Grampian outliers: implications for Caledonian orogenic basin development and the northward extension of the Midland Valley Basin. *J. Geol. Soc.* **178**, jgs2020–jgs2141 (2021).
90. McKellar, Z., Hartley, A. J., Morton, A. C. & Frei, D. A multidisciplinary approach to sediment provenance analysis of the late Silurian–Devonian Lower Old Red Sandstone succession, northern Midland Valley Basin, Scotland. *J. Geol. Soc.* **177**, 297–314 (2020).
91. Phillips, E., Smith, R., Stone, P., Pashley, V. & Horstwood, M. Zircon age constraints on the provenance of Llandovery to Wenlock sandstones from the Midland Valley terrane of the Scottish Caledonides. *Scott. J. Geol.* **45**, 131–146 (2009).
92. Morton, A. C., Chisholm, J. I. & Frei, D. Provenance of Carboniferous sandstones in the central and southern parts of the Pennine Basin, UK: evidence from detrital zircon ages. *Proc. Yorks. Geol. Soc.* **63**, https://doi.org/10.1144/pygs2020-010 (2021).
93. Hallsworth, C., Morton, A., Claoué-Long, J. & Fanning, C. Carboniferous sand provenance in the Pennine Basin, UK: constraints from heavy mineral and detrital zircon age data. *Sediment. Geol.* **137**, 147–185 (2000).

94. Bevins, R. E. et al. Constraining the provenance of the Stonehenge 'Altar Stone': evidence from automated mineralogy and U–Pb zircon age dating. *J. Archaeol. Sci.* **120**, 105188 (2020).
95. Clarke, A. J. I. Supplementary information 1-3, https://doi.org/10.6084/m9.figshare.30690479 (2025).
96. Waldron, J. W. F. et al. Ganderia–Laurentia collision in the Caledonides of Great Britain and Ireland. *J. Geol. Soc.* **171**, 555–569 (2014).
97. Nordsvan, A. R., Kirscher, U., Kirkland, C. L., Barham, M. & Brennan, D. T. Resampling (detrital) zircon age distributions for accurate multidimensional scaling solutions. *Earth Sci. Rev.* **204**, 103149 (2020).

Acknowledgements

This work was funded by the Timescales of Mineral Systems Group at Curtin University. Instruments in the JdLC, Curtin University, were supported by AuScope and the National Collaborative Research Infrastructure Strategy. The authors thank B. McDonald and K. Rankenburg for assistance during LA–ICP–MS analysis. Stream sediment samples SH1–SH4 were collected from public ground without accessing private land. All sampling followed Environment Agency guidance and adhered to the Geological Society of London's Code for Geological Fieldwork. No specific permissions were required. We thank Gary O'Sullivan and two anonymous reviewers for their comments, which improved this contribution.

Author contributions

Anthony J.I. Clarke led the methodology, investigation, data curation, formal analysis, visualisation, writing of the original draft, writing and editing, and project administration. He also contributed equally with Christopher L. Kirkland to the conceptualisation of the study. Christopher L. Kirkland contributed to the conceptualisation, methodology, investigation, formal analysis, and writing and editing of the manuscript. He also led the acquisition of funding for the project.

Competing interests

The authors declare no competing interests.

Additional information

Supplementary information The online version contains supplementary material available at https://doi.org/10.1038/s43247-025-03105-3.

Correspondence and requests for materials should be addressed to Anthony J. I. Clarke.

Peer review information *Communications Earth & Environment* thanks Gary O'Sullivan, Adrian M. Hall and the other anonymous reviewer(s) for their contribution to the peer review of this work. Primary handling editors: Yuan Shang and Alireza Bahadori. A peer review file is available.